

Upper Critical Field of Pressure-Induced Superconductor EuFe_2As_2

Nobuyuki Kurita^{1,2}, Motoi Kimata^{1,2}, Kota Kodama^{1,3}, Atsushi Harada¹, Megumi Tomita¹, Hiroyuki S. Suzuki¹, Takehiko Matsumoto¹, Keizo Murata⁴, Shinya Uji^{1,2,3}, and Taichi Terashima^{1,2}

¹*National Institute for Materials Science, Tsukuba, Ibaraki 305-0003, Japan*

²*JST, Transformative Research-Project on Iron Pnictides (TRIP), Chiyoda, Tokyo 102-0075, Japan*

³*Graduate School of Pure and Applied Sciences, University of Tsukuba, Ibaraki 305-0003, Japan*

⁴*Division of Molecular Materials Science, Graduate School of Science, Osaka City University, Osaka 558-8585, Japan*

(Dated: February 5, 2022)

We have carried out high-field resistivity measurements up to 27 T in EuFe_2As_2 at $P = 2.5$ GPa, a virtually optimal pressure for the P -induced superconductivity, where $T_c = 30$ K. The $B_{c2}-T_c$ phase diagram has been constructed in a wide temperature range with a minimum temperature of 1.6 K ($\approx 0.05 \times T_c$), for both $B \parallel ab$ (B_{c2}^{ab}) and $B \parallel c$ (B_{c2}^c). The upper critical fields $B_{c2}^{ab}(0)$ and $B_{c2}^c(0)$, determined by the onset of resistive transitions, are 25 T and 22 T, respectively, which are significantly smaller than those of other Fe-based superconductors with similar values of T_c . The small $B_{c2}(0)$ values and the $B_{c2}(T)$ curves with positive curvature around 20 K can be explained by a multiple pair-breaking model that includes the exchange field due to the magnetic Eu^{2+} moments. The anisotropy parameter, $\Gamma = B_{c2}^{ab}/B_{c2}^c$, in EuFe_2As_2 at low temperatures is comparable to that of other “122” Fe-based systems.

PACS numbers: 74.25.Op, 74.25.Dw, 74.25.F-, 74.62.Fj

The discovery of superconductivity in $\text{LaFeAs}(\text{O},\text{F})$ at $T_c = 26$ K¹ has inspired experimental and theoretical research on a group of FeAs-layered superconductors (SCs).² Basically, Fe-based high- T_c superconductivity^{3–5} occurs when the antiferromagnetic (AF) order in the mother compounds is suppressed by means of carrier doping,¹ application of pressure (P),⁶ or isovalent substitution.⁷ As compared to other methods in studying such interplay between magnetism and superconductivity, pressure experiments have a significant advantage in that they are free from random impurity potentials that may distort the underlying physics of the low-lying energy states. Among the various crystal structures, tetragonal ThCr_2Si_2 -type (“122”) compounds have been investigated more intensively owing to the availability of highly-pure stoichiometric single crystals. In particular, AFe_2As_2 ($A = \text{Sr}, \text{Eu}$) exhibits P -induced bulk superconductivity with T_c of order 30 K.^{6,8,9} In contrast, superconductivity under hydrostatic pressure is not exhibited by CaFe_2As_2 ,¹⁰ and its occurrence in BaFe_2As_2 has not been established definitively.^{8,11}

A fundamental characteristic of SCs is the upper critical field B_{c2} . B_{c2} has its roots in the breakdown of Cooper pairs; hence, the $B_{c2}-T_c$ phase diagram provides important insights into the pairing mechanism of high- T_c superconductivity. Thus far, to our knowledge, there has been no reports on B_{c2} for P -induced Fe-based SCs at low temperatures. This is mainly attributed to the difficulty in conducting high-pressure experiments on high- T_c SCs under a high-field. In the case of SrFe_2As_2 ($T_c = 30$ K at 4.2 GPa), a field of 8 T brings about a small reduction in T_c (i.e., to 27 K) for $B \parallel ab$.¹³ Assuming an orbitally limited case,¹² B_{c2} ($T = 0$ K) could exceed 60 T.¹³ However, the low-temperature region of the B_{c2} curve, where paramagnetic and/or multiband effects may play important roles,¹⁴ has not been investigated.

In the case of EuFe_2As_2 ($T_c = 30$ K at ~ 2.5 GPa), B_{c2} is relatively small, i.e., ~ 16 T between 5 K and 10 K,⁹ and hence can be traced down to very low temperatures. EuFe_2As_2 is unique in that the localized Eu^{2+} moments exhibit an AF order below 20 K^{15–19} in addition to an AF order arising from the FeAs layers at $T_0 \sim 190$ K. T_N of the Eu^{2+} moments is insensitive to pressure, and the AF order occurs in the P -induced superconducting state as evidenced by magnetic and heat capacity measurements under high-pressure.^{9,20–22} Despite the AF order, which is produced by a weak interlayer interaction, the dominant interaction among the Eu^{2+} moments is the intralayer ferromagnetic (FM) interaction, and hence the FM alignment of the Eu^{2+} moments is easily achieved by the application of 1–2 T even below T_N at ambient pressure as well as under high pressure.^{9,18–20,23,24} Thus, EuFe_2As_2 provides an excellent opportunity where a long-standing issue of the interplay between superconductivity and magnetism can be studied in a high- T_c material using high-quality single crystals.

In this report, we present the $B_{c2}-T_c$ phase diagram of EuFe_2As_2 at a pressure of 2.5 GPa and minimum temperature of 1.6 K via high-field resistivity measurements up to 27 T, and discuss the origin of the distinctive B_{c2} curves.

Single crystals of EuFe_2As_2 were prepared via the Bridgman method from a stoichiometric mixture of the constituent elements. The samples analyzed in this study were obtained from the same batch (residual resistivity ratio $RRR = 7$) as that used in Refs. 9, 21 and 23. The resistivity of two samples, denoted by #1 and #2, was simultaneously measured at $P = 2.5$ GPa via an ac four-probe method in a ^4He cryostat ($T \geq 1.6$ K). Sample #1 (#2) was aligned with the ab -plane (c -axis) parallel to the longitudinal direction of a hybrid-type piston cylinder pressure cell²⁵ for $B \parallel ab$ ($\parallel c$) measurements. For both

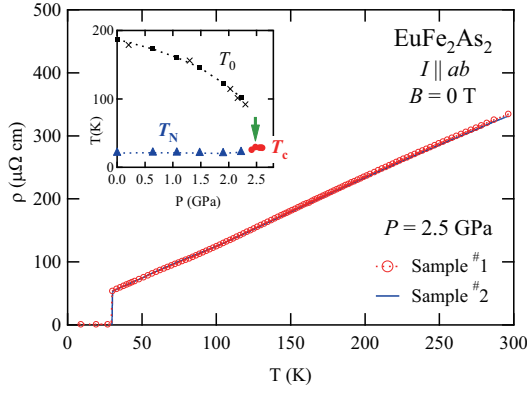


FIG. 1: (Color online) ρ vs T for EuFe_2As_2 at $P = 2.5$ GPa for samples #1 and #2 in the absence of applied field. The direction of current I is $I \parallel ab$. The inset illustrates the T - P phase diagram of EuFe_2As_2 .²⁹ T_0 and T_N denote the temperatures of the AF order arising from the FeAs layers and localized Eu^{2+} moments, respectively. The solid circles denote T_c determined under the criterion $\rho = 0$. The crosses denote the values obtained from Ref. 20.

samples, the magnetic field was applied along the piston cylinder axis in a direction perpendicular to that of the current. To generate hydrostatic pressure, Daphne 7474 (Idemitsu Kosan) oil, which remains in the liquid state up to 3.7 GPa at room temperature,²⁶ was used as the pressure-transmitting medium. The samples were gradually cooled at an average rate of 0.5 K/min. The pressure was calibrated at 4.2 K by the resistance change of a Manganin wire.⁹ Magnetic fields up to 27 T were produced by a water-cooled resistive magnet installed at the Tsukuba Magnet Laboratory, National Institute for Materials Science. A 17-T superconducting magnet was used for preliminary resistivity studies. In this study, the magnetic field B denotes an externally applied field, and the magnetization within a sample (up to $\sim 0.9 \text{ T}^{23}$) is neglected.

Figure 1 shows the temperature dependence of the resistivity, $\rho(T)$, for the two samples, #1 and #2, at $P = 2.5$ GPa in the absence of an applied field. For both samples, ρ exhibits virtually T -linear dependence in the broad temperature range above T_c without any anomaly due to the AF order of the FeAs layers. This observation is consistent with the phase diagram shown in the inset:^{20,29} $P = 2.5$ GPa is just above the critical pressure P_c , where $T_0 \rightarrow 0$, as indicated by the arrow. Similar $\rho \sim T$ behavior was also reported in several optimally doped Fe-based SCs.^{27,28} However the reason for such behavior has not been verified thus far. Both samples exhibit a sharp transition to zero resistivity at $T_c = 30$ K; the reentrant-like behavior as reported in Ref. 20 is not observed for either sample at this pressure. Our previous work²¹ indicates that reentrant-like behavior may be observed for $P < P_c$ but not for $P > P_c$ (as long as P is not far from P_c) in our single crystals. Since both

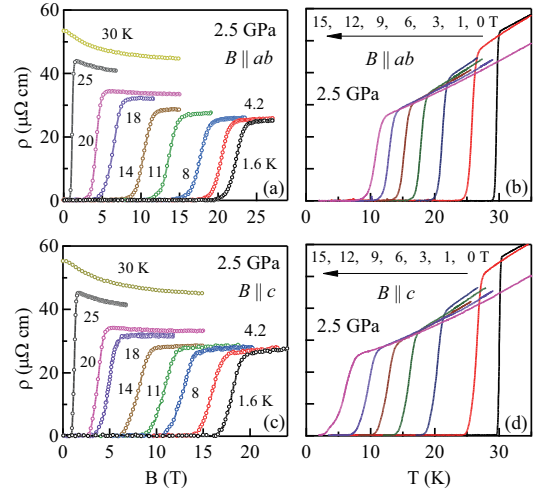


FIG. 2: (Color online) (a) ρ vs B and (b) ρ vs T for $B \parallel ab$ (sample #1) and (c) ρ vs B and (d) ρ vs T for $B \parallel c$ (sample #2) in EuFe_2As_2 at $P = 2.5$ GPa.

T_c and B_{c2} attain maximum values at $P \approx P_c$, followed by a monotonic decrease with increasing P .²⁹ B_{c2} determined at 2.5 GPa in this study is expected to be close to its maximum value.

Figure 2(a)-(d) shows the resistivity of EuFe_2As_2 at 2.5 GPa as a function of B and T for the two orientations $B \parallel ab$ and $B \parallel c$. A magnetic field of 27 T is sufficient to recover the normal state at the minimum temperature, 1.6 K ($\approx 0.05 \times T_c$), for both orientations. Using the data in Fig. 2(a) and (b), the B_{c2} - T_c phase diagram of EuFe_2As_2 is constructed for $B \parallel ab$ at 2.5 GPa, as shown in Fig. 3. Three sets – B_{c2} , B_{c2}^{on} (onset), and B_{c2}^x ($x=0$ and 50, $x\%$ of the normal state resistivity ρ_n) – are plotted, and their definitions are illustrated in the inset. The solid and open symbols are obtained from the $\rho(B)$ and $\rho(T)$ measurements, respectively. B_{c2}^0 is consistent with the previous result (\times) obtained from the ac- χ measurement for $B \parallel ab$.⁹ Note that all the curves of B_{c2} for $B \parallel ab$ (B_{c2}^{ab}) obtained under different criteria exhibit qualitatively similar T -dependence. The same is also true for B_{c2} for $B \parallel c$ (B_{c2}^c), as shown in Fig. 4(a). T_N at zero field is indicated by an arrow in Figs. 3 and 4. However, we note that, since the AF order of the Eu^{2+} moments is destroyed by an applied field of ~ 1 T,⁹ the B_{c2} curves for both $B \parallel ab$ and $B \parallel c$ are in the paramagnetic or field-induced FM state of the Eu^{2+} moments.

A distinctive feature, the concave (upward) curvature of B_{c2}^{ab} around 20 K, has not been reported in other Fe-based SCs without localized magnetic ions. Therefore, it is likely related to the magnetic state of the Eu^{2+} moments. Similar concave $B_{c2}(T)$ curves have been reported in Chevrel-phase compounds such as $(\text{Eu}, M)\text{Mo}_6\text{S}_8$ ($M = \text{Sn}$,³⁰ La ,³¹ etc.) and EuMo_6S_8 under pressure.³² In these systems, the conduction electrons are subjected to an exchange field B_J in addition to an

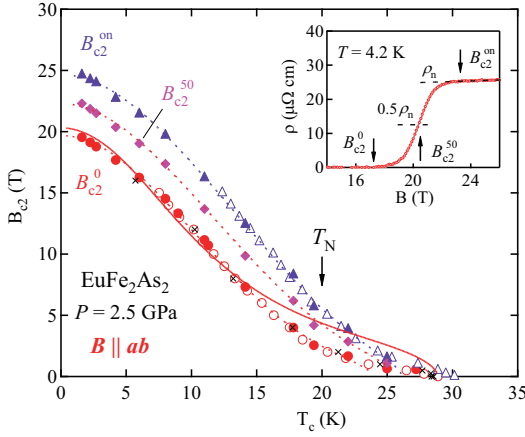


FIG. 3: (Color online) B_{c2} – T_c phase diagram of EuFe_2As_2 for $B \parallel ab$ at 2.5 GPa. The values of B_{c2} are determined under three different criteria, as illustrated for $\rho(B)$ data at 4.2 K (inset). The solid or open symbols denote B_{c2} determined from $\rho(B)$ and $\rho(T)$ measurements, respectively. The solid and dashed curves are fits to Eq.(1). \times denotes the previous B_{c2}^0 result deduced from an ac- χ measurement for $B \parallel ab$ ⁹. The arrow indicates T_N of Eu^{2+} moments in the superconducting state in the absence of an applied field at 2.6 GPa⁹.

applied field via AF coupling with the Eu^{2+} localized magnetic moments. Note that the concave curvature is an indication of the negative sign of B_J ; B_J is antiparallel to the applied field.^{32,33} Within a multiple pair-breaking picture, B_{c2} in the dirty limit of three-dimensional SCs with negative B_J can be expressed by^{12,34}

$$\ln \frac{1}{t} = \left(\frac{1}{2} + \frac{i\lambda_{\text{so}}}{4\gamma} \right) \times \Psi \left(\frac{1}{2} + \frac{h + i\lambda_{\text{so}}/2 + i\gamma}{2t} \right) + \left(\frac{1}{2} - \frac{i\lambda_{\text{so}}}{4\gamma} \right) \times \Psi \left(\frac{1}{2} + \frac{h + i\lambda_{\text{so}}/2 - i\gamma}{2t} \right) - \Psi \left(\frac{1}{2} \right)$$

$$\gamma = [\alpha^2(h + h_J)^2 - \lambda_{\text{so}}^2]^{\frac{1}{2}} \quad (1)$$

where Ψ and λ_{so} are the digamma function and spin-orbit scattering parameter, respectively. The magnetic scattering parameter λ_m used in the complete formula^{12,34} is typically ignored for simplicity.^{32,35} The Maki parameter α is defined as $\sqrt{2} B_{c2}^*/B_p$, using the orbital critical field B_{c2}^* at $T=0$ and the Pauli-Clogston paramagnetic limit B_p ³⁶. Reduced units $-t = T/T_c$, $h = 0.281 B_{c2}/B_{c2}^*$, and $h_J = 0.281 B_J/B_{c2}^*$ are employed. We assume $B_J = \beta M$ (β : constant), where the magnetization M is modeled within a molecular-field approximation.³⁷ To simplify the following discussions, α for $B \parallel ab$ is set to 3, a typical value for “122” systems.

The solid curve in Fig. 3 was calculated from Eq.(1) for B_{c2}^0 data with T_c set to the experimental value $T_c = 29$ K. The fit yields a parameter set $(\lambda_{\text{so}}, \beta) = (7.9, -187)$. $\beta = -187$ indicates that the maximum of $|B_J|$, B_J^m , is around 168 T. The fit captures the qualitative character-

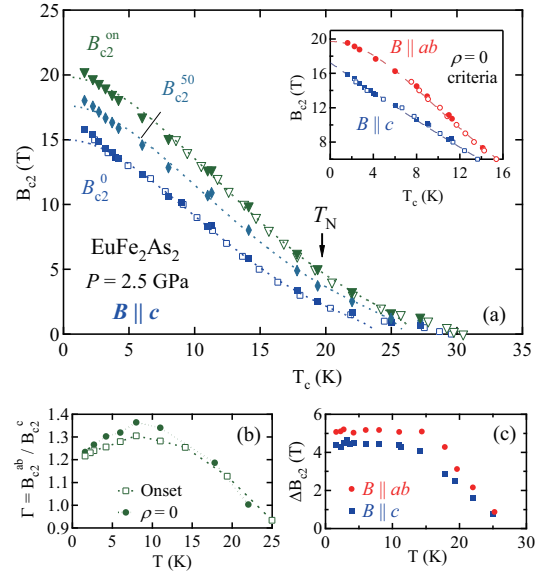


FIG. 4: (Color online) (a) B_{c2} – T_c phase diagram of EuFe_2As_2 for $B \parallel c$ at 2.5 GPa. The solid and open symbols denote B_{c2} deduced from $\rho(H)$ and $\rho(T)$ data, respectively. The dashed curves are fits to Eq.(1). The inset shows B_{c2}^0 vs T_c for $B \parallel ab$ and $B \parallel c$. The dashed curves are fits for $T=0$ extrapolation (see text). (b) T -variation of an anisotropy parameter, $\Gamma = B_{c2}^{ab}/B_{c2}^c$, determined by the onset and zero-resistivity. (c) T -dependence of the superconducting transition width, $\Delta B_{c2} (= B_{c2}^{\text{on}} - B_{c2}^0)$, for $B \parallel ab$ and $B \parallel c$.

istics of the experimental B_{c2}^0 curve satisfactorily, especially the positive curvature below $T_N = 20$ K, and shows that the low value of B_{c2} (compared to other Fe-based SCs with similar T_c values) is due to the large B_J , which is a consequence of a large Eu^{2+} magnetization due to the field-induced FM alignment of the Eu^{2+} moments. However, its deviation from the experimental curve is also noticeable at low fields near T_c . This disagreement probably indicates that the phase diagram in this T -range is affected by a subtle competition between superconductivity and magnetic fluctuations, and it is beyond the scope of Eq.(1), which assumes a homogeneous B_J produced by paramagnetic spins. Since the dominant interaction among the Eu^{2+} moments is the intralayer FM interaction,^{18,19,23,24} the FM fluctuations develop when T is lowered to T_N , as evidenced by the enhancement of the magnetic susceptibility as $T \rightarrow T_N$.^{9,19,23} Such FM fluctuations may be detrimental to superconductivity. One way to phenomenologically overcome this problem and to improve the fit in a T -range not close to T_c is to use a reduced value of T_c . Thus, the three dotted curves are calculated using the reduced T_c value. They reproduce the experimental curves excellently over the entire T -range, with a minimum temperature of 1.6 K. For B_{c2}^0 , we assumed $(\lambda_{\text{so}}, \beta, T_c) = (2.7, -83, 24 \text{ K})$, where $B_J^m \sim 75$ T. Here, it may be worthwhile to compare the parameters with those of the Chevrel compounds. The compari-

son revealed that the obtained λ_{so} is comparable to that found in the Chevrel-type Eu compounds,^{32,35} and B_J^m in EuFe₂As₂ is a few times greater than that reported in the Chevrel-type Eu compounds.^{32,35} We note that the concave curvature of B_{c2} in EuFe₂As₂ essentially differs from the positive curvatures often observed in highly two-dimensional SCs such as high- T_c cuprates. In the latter, the curvature is highly dependent on what criterion is chosen to define B_{c2} , and it is most likely affected by the vortex lattice phase transitions, i.e. from a vortex-liquid state to a vortex-solid state.³⁸

Figure 4(a) shows the B_{c2} - T_c phase diagram of EuFe₂As₂ for $B \parallel c$ at 2.5 GPa,³⁹ determined in the same manner as that used for B_{c2}^{ab} . A concave curvature around 20 K is also visible for the B_{c2}^c curves. The dashed curves are calculated using the parameters comparable to those used for B_{c2}^{ab} , i.e., for B_{c2}^0 , the fit gives $(\alpha, \lambda_{so}) = (1.9, 2.6)$ when we assume $(\beta, T_c) = (-83, 24 \text{ K})$, identical to the values used for B_{c2}^{ab} . The calculated curves tend to saturate below 3 K, whereas the experimental curves appear to increase linearly as T decreases to zero. The unsaturation of B_{c2}^c has been observed in other Fe-based SCs,^{14,40–42} and it has been explained using a two-band model. Figure 4(b) shows the anisotropy ratio, $\Gamma = B_{c2}^{ab} / B_{c2}^c$, calculated from $B_{c2}^0(T)$ and $B_{c2}^{on}(T)$. In spite of the quasi-two-dimensional layered structure in EuFe₂As₂, we obtain a small value of Γ , ranging between 0.9 and 1.4, which is comparable to that obtained for other “122” compounds.^{40–43} In contrast to the monotonic decrease in Γ with decreasing T in other “122” compounds, Γ in EuFe₂As₂ exhibits a broad maximum at around 8 K, which is likely ascribed to the presence of the B_J .

In order to compare the magnitude of $B_{c2}(0)$ with that of other Fe-based SCs, we estimate it by extrapolating the low- T data to $T = 0$, as shown by the dashed curves in the inset of Fig. 4(a). For the extrapolations, an empirical expression, $B_{c2}(t) = B_{c2}(0)(1 - t^2)/(1 + t^2)$,⁴⁴ and a linear fit are used for B_{c2}^{ab} and B_{c2}^c , respectively. We obtain $B_{c2}^{ab}(0) = 24.7 \text{ T}$ and 19.7 T and $B_{c2}^c(0) = 21.5 \text{ T}$ and 17.2 T for B_{c2}^{on} and B_{c2}^0 , respectively. $B_{c2}(0)$ in EuFe₂As₂ is significantly lower than $B_{c2}(0) > 50 \text{ T}$ in other Fe-based SCs at $T_c = 20 - 30 \text{ K}$.^{14,40–42} The width of the superconducting transition, $\Delta B (= B_{c2}^{on} - B_{c2}^0)$, increases as T decreases to 15 K for both $B \parallel ab$ and $B \parallel c$ [Fig. 4(c)]. Below 15 K, ΔB is virtually T -independent, as reflected by the parallel-shifts of the $\rho(B)$ curves in Fig. 2(a) and (c). The T -dependence may correlate with the development of M ; M at $B = B_{c2}(T)$ increases rapidly as T decreases from T_c , but it is virtually saturated below $\sim 15 \text{ K}$.¹⁹ At 1.6 K, ΔB is estimated as 5.1 T and 4.4 T for $B \parallel ab$ and $B \parallel c$, respectively. The relatively narrow transition width at low T , which is also observed in Ba(Fe,Co)₂As₂,^{42,43} signifies a strong vortex pinning force in EuFe₂As₂.

In conclusion, we carried out high-field resistivity measurements up to 27 T for EuFe₂As₂ at 2.5 GPa, and we constructed the B_{c2} - T_c phase diagram down to a minimum temperature of 1.6 K. Our analysis was based on a multiple pair-breaking model, and it revealed that the distinctive B_{c2} curves with positive curvature and the reduced B_{c2} values can be attributed to the substantial negative exchange field from the Eu²⁺ moments. The low temperature anisotropy at 1.6 K, $\Gamma = 1.2$, is comparable to the results obtained for other “122” systems.

-
- ¹ Y. Kamihara *et al.*, J. Am. Chem. Soc. **130**, 3296 (2008).
 - ² For recent reviews, see K. Ishida *et al.*, J. Phys. Soc. Jpn. **78**, 062001 (2009) and D. C. Johnston, Advances in Physics **59**, 803 (2010).
 - ³ H. Kito *et al.*, J. Phys. Soc. Jpn. **77**, 063707 (2008).
 - ⁴ Z.-A. Ren *et al.*, Chin. Phys. Lett. **25**, 2215 (2008).
 - ⁵ C. Wang *et al.*, Europhys. Lett. **83**, 67006 (2008).
 - ⁶ P. L. Alireza *et al.*, J. Phys.: Condens. Matter **21**, 012208 (2008).
 - ⁷ Z. Ren *et al.*, Phys. Rev. Lett. **102**, 137002 (2009).
 - ⁸ K. Matsubayashi *et al.*, J. Phys. Soc. Jpn. **78**, 073706 (2009).
 - ⁹ T. Terashima *et al.*, J. Phys. Soc. Jpn. **78**, 083701 (2009); **78**, 118001 (2009); Physica C **470**, S443 (2010).
 - ¹⁰ W. Yu *et al.*, Phys. Rev. B **79**, 020511(R) (2009).
 - ¹¹ T. Yamazaki *et al.*, Phys. Rev. B **81**, 224511 (2010).
 - ¹² N. R. Werthamer *et al.*, Phys. Rev. **147**, 295 (1966).
 - ¹³ H. Kotegawa *et al.*, J. Phys. Soc. Jpn. **78**, 013709 (2009).
 - ¹⁴ F. Hunte *et al.*, Nature **453**, 903 (2008).
 - ¹⁵ H. Raffius *et al.*, J. Phys. Chem. Solids **54**, 135 (1993).
 - ¹⁶ H. S. Jeevan *et al.*, Phys. Rev. B **78**, 052502 (2008).
 - ¹⁷ Z. Ren *et al.*, Phys. Rev. B **78**, 052501 (2008).
 - ¹⁸ Y. Xiao *et al.*, Phys. Rev. B **80**, 174424 (2009).
 - ¹⁹ S. Jiang *et al.*, N. J. Phys. **11**, 025007 (2009).
 - ²⁰ C. F. Miclea *et al.*, Phys. Rev. B **79**, 212509 (2009).
 - ²¹ N. Kurita *et al.*, arXiv: 1008.0684 (2010), to appear in J. Phys: Conf. Ser. (2011).
 - ²² K. Matsubayashi *et al.*, arXiv:1007.2889 (2010).
 - ²³ T. Terashima *et al.*, J. Phys. Soc. Jpn. **79**, 103706 (2010).
 - ²⁴ Y. Xiao *et al.*, Phys. Rev. B **81**, 220406 (R) (2010).
 - ²⁵ Y. Uwatoko *et al.*, Physica C **329-333**, 1658 (2003).
 - ²⁶ K. Murata *et al.*, Rev. Sci. Instrum. **79**, 085101(2008).
 - ²⁷ R. H. Liu *et al.*, Phys. Rev. Lett. **101**, 087001 (2008).
 - ²⁸ M. Gooch *et al.*, Phys. Rev. B **79**, 104504 (2009).
 - ²⁹ N. Kurita *et al.*, unpublished.
 - ³⁰ Ø. Fischer *et al.*, J. Phys. C **8**, L474 (1975).
 - ³¹ M. S. Torikachvili and M. B. Maple, Solid State Commun. **40**, 1 (1981).
 - ³² M. Decroux *et al.*, Phys. Rev. Lett. **52**, 1563 (1984).
 - ³³ V. Jaccarino and M. Peter, Phys. Rev. Lett. **9**, 290 (1962).
 - ³⁴ Ø. Fisher, Helv. Phys. Acta **45**, 331 (1972).
 - ³⁵ C. Rossel *et al.*, J. Appl. Phys. **57**, 3099 (1985).
 - ³⁶ B. S. Chandrasekhar, Appl. Phys. Lett. **1**, 7 (1962); A. M. Clogston, Phys. Rev. Lett. **9**, 266 (1962).
 - ³⁷ The model reproduces experimental c -axis magnetization satisfactorily.²³ The anisotropy of magnetization is small, except for a low- T and low- B region;¹⁹ hence, we use the

same model for both $B \parallel ab$ and $B \parallel c$.

³⁸ Y. Ando *et al.*, Phys. Rev. **B 60**, 12475 (1999).

³⁹ There is discrepancy between the present and previous B_{c2}^c data. The latter was determined from ac- χ .⁹ This could be due to the difference in the applied pressure and/or sample variations. In this study, ρ was simultaneously measured using the two samples from the same piece.

⁴⁰ H. Q. Yuan *et al.*, Nature **457**, 565 (2009).

⁴¹ S. A. Baily *et al.*, Phys. Rev. Lett. **102**, 117004 (2009).

⁴² M. Kano *et al.*, J. Phys. Soc. Jpn. **78**, 084719 (2009).

⁴³ A. Yamamoto *et al.*, Appl. Phys. Lett. **94**, 062511 (2009)

⁴⁴ A. Leitner *et al.*, Phys. Rev. **B 62**, 1408 (2000).